Elucidating the mechanisms of rapid O_3 increase in North China Plain during COVID-19 lockdown period

Rui Li[a *], Yining Gao[a], Gehui Wang[a **]

[a] *Key Laboratory of Geographic Information Science of the Ministry of Education, School of Geographic Sciences, East China Normal University, Shanghai, 200241, PR China*

*** Correspondence to:**

Prof. Li (rli@geo.ecnu.edu.cn) and Prof. Wang (ghwang@geo.ecnu.edu.cn)

Abstract

Ozone (O_3) levels in North China Plain (NCP) suffered from rapid increases during the COVID-19 period. Many previous studies have confirmed more rapid NO_x reduction compared with VOCs might be responsible for the O_3 increase during this period, while the comprehensive impacts of each VOC species and NO_x on ambient O_3 and their interactions with meteorology were not revealed clearly. To clarify the detailed reasons for the O_3 increase, a continuous campaign was performed in a typical industrial city of NCP. Meanwhile, the machine-learning technique and the box model were employed to reveal the mechanisms of O_3 increase from the perspective of meteorology and photochemical process, respectively. The result suggested that the ambient O_3 level in Tangshan increased from 18.7 ± 4.63 to 45.6 ± 8.52 μg/m^3 (143%) after COVID-19 lockdown, and the emission reduction and meteorology contributed to 77% and 66% of this increment, respectively. The higher wind speed (WS) coupled with regional transport played a significant role on O_3 increase (30.8 kg/s). The O_3 sensitivity verified that O_3 production was highly volatile organic compounds (VOC)-sensitive (Relative incremental reactivity (RIR): 0.75), while the NO_x showed the negative impact on O_3 production in Tangshan (RIR: -0.59). It suggested that the control of VOCs rather than NO_x might be more effective in reducing O_3 level in Tangshan because it was located on the VOC-limited regime. Besides, both of ozone formation potential (OFP) analysis and observation-based model (OBM) demonstrated that the alkenes (36.3 ppb) and anthropogenic oxygenated volatile organic compounds (OVOCs) (15.2 ppb) showed the higher OFP compared with other species, and their reactions released a large number of HO_2 and RO_2 radicals. Moreover, the concentrations of these species did not experience marked decreases after COVID-19 lockdown, which were major contributors to O_3 increase during this period. This study underlines the necessity of priority controlling alkenes and OVOCs, which will benefit not just NCP but also other regions in China.

Summary

The major aims of our study are to reveal the detailed mechanisms for O_3 increase in North China Plain (NCP). It was well known that the O_3 level experienced dramatic increase in NCP even in East China during COVID-19 period. Although many previous studies have confirmed more rapid NO_x reduction compared with VOCs might be responsible for the O_3 increase, we believed the drastic O_3 increase might be not caused by a single factor. Some other factors should be further explored. To date, the comprehensive impacts of each VOC species and NO_x on ambient O_3 and their interactions with meteorology were not revealed clearly. Based on the detailed analysis in our study, we demonstrated OVOCs and alkenes showed the higher OFP compared with other species, and their reactions released a large number of HO_2 and RO_2 radicals, which was responsible for the O_3 increase during this period. The natural experiment gave us many policy implications about O_3 pollution control. For instance, the collaborative controls VOC and NO_x must be seriously performed in the near future. Moreover, more efforts are needed for the control of alkenes and OVOCs.

Although we only performed the observation at a single city, the policy implication of our study was not limited to the local focus. At first, Tangshan possessed many energy-intensive industries including coal-fired power plants, non-ferrous smelting industries, and cement factories. It is a typical region to reveal O_3 formation mechanisms and radical chemistry because it could reflect the overall characteristics of NCP. Moreover, Li et al. (2019) revealed the emissions of alkenes and OVOCs derived from paint use and chemical industry across China experienced rapid increases since 2010 and will keep the trend in the near future. Therefore, our policy implication will benefit not just NCP but also other regions in China.

1. Introduction

In December 2019, a tragic coronavirus (COVID-19) has spread worldwide causing over 6.33 million deaths as of this writing. In order to combat the further spread of COVID-19, Chinese government imposed many unconventional and stringent control measures. Nearly all of the provinces launched full-lockdown responses from 23 January to the early February, 2020.

During this period, many strict lockdown measures including the shutdown of industries and non-essential businesses, curfews, and quarantines necessarily resulted in the reduction of anthropogenic pollutant emissions. In turn, the dramatic decreases of primary emissions led to

marked changes of air pollutant concentrations. For instance, Zhao et al. (2020) reported that the concentrations of $PM_{2.5}$, PM_{10}, SO_2, and NO_2 across China decreased by 13.7%, 21.8%, 4.6%, and 46.1%, respectively. Compared with aerosols and gaseous precursors, the concentration decreases of secondary inorganic ions were not remarkable. Li et al. (2021b) confirmed that the sulfate level in Tangshan only decreased by 6% after COVID-19 lockdown. Surprisingly, marginal increases in O_3 were observed in many cities across East China (e.g., Wuhan, Shanghai), which seems to be in contrast to the changes of most other air pollutants (Saha et al., 2022; Venter et al., 2020). As a photochemical product, elevated O_3 levels often enhanced the atmospheric oxidation capacity (AOC) and exerted hazardous impacts on human health and ecosystem (Liu et al., 2022). The exploration of key driving forces for O_3 pollution has become a hot topic for scientific community. During COVID-19 period, VOCs and NO_x levels experienced substantial changes due to strict emission control measures, and both of these compositions further affected radical chemistry and O_3 change (Goldberg et al., 2022; Nussbaumer et al., 2022). It provided us an unprecedent opportunity to fill the knowledge gap about the responses of O_3 and radical chemistry to the drastic changes of precursor emissions, which facilitated the optimization of emission control strategy.

It was well known that the O_3 level was often affected by the comprehensive impacts of meteorological conditions, precursor emissions, and photochemical processes (Li et al., 2022). Therefore, it is essential to distinguish the contributions of meteorological parameters and emission change firstly, and then to figure out the O_3 formation mechanisms and sensitivity. Unfavorable meteorological condition was often considered to be the key factor for the O_3 increase (Yin et al., 2021; Zhang et al., 2022b). Gong et al. (2018) revealed that daily maximum temperature was major driving factor responsible for the national O_3 pollution. Besides, RH, WS, and solar radiation also played significant roles on the O_3 pollution especially in summer and autumn (Chen et al., 2019). To date, some researchers have employed chemical transport models (CTMs) and statistical models to distinguish the contributions of meteorological conditions and emission changes to O_3 pollution. Zhao et al. (2020) utilized Weather Research and Forecasting (WRF) model and the Community Multiscale Air Quality (CMAQ) model to reveal that the contribution of meteorological factor to O_3 increase in some megacities (e.g., Beijing, Shanghai, Guangzhou) during COVID-19 period ranged from 15% to 65%. Later on, Wang et al. (2020b) applied machine-learning models to assess the contribution of meteorological condition to O_3 pollution in six megacities of China and the result

was in good agreement with study based on CTMs. Unfortunately, these pioneering studies did not analyze the independent impact of each meteorological parameter on O_3 increase during the pandemic and the dominant meteorological factor were scarcely revealed. Furthermore, the contribution of regional transport to O_3 pollution at the fine scale was also less quantified. Compared with the simple separation of meteorology and emission, the detailed assessment was favorable to the effective implementation of O_3 pollution prevention policy under the circumstance of different meteorological conditions.

Apart from the impact of meteorological factors, the photochemical processes played important roles on the ambient O_3. As a novel technique to analyze the reasons of O_3 pollution, OBM-master chemical mechanism (MCM) has been widely applied to investigate O_3-VOC-NO_x relationships and radical chemistry. The method about O_3 sensitivity to VOCs and NO_x also have been established to uncover O_3 formation mechanisms and pollution control strategies. Up to date, many studies have employed this advanced technique to determine the key formation pathways of ambient O_3. Liu et al. (2019) analyzed the budget of ambient O_3 in Hong Kong in the autumn of 2007, 2013, and 2016 and found the contribution of HO_2 + NO only accounted for 56 ± 1 % of the total O_3 production. However, Liu et al. (2022) estimated that the contribution ratio of HO_2 + NO reached 68 ± 4 % in the autumn of Xiamen. The O_3 formation pathway varied greatly in different cities and seasons, which might be strongly dependent on primary emission, the ratio of volatile organic compounds and nitrogen oxides (VOC/NO_x), AOC, and radical chemistry. Up to date, most of the current studies focused on the O_3 formation mechanisms and radical chemistry in summer and autumn, while few studies clarified the reasons for O_3 pollution events in winter. In fact, winter also suffered from substantial increase of O_3 concentration such as COVID-19 period. Unfortunately, only Zhang et al. (2022a) applied this method to determine the source-sink mechanism of atmospheric O_3 during COVID-19 period. Moreover, this study ignored the contributions of alkanes and most alkenes to O_3 pollution. Although the OFP value of alkanes was generally lower than alkenes and oxygenated volatile organic compounds (OVOCs), the absolute concentrations of ambient alkanes were often largely higher than alkenes and OVOCs. Thus, the neglect of alkanes might underestimate the ozone production and could mislead the diagnosis of ozone sensitivity regimes. In addition, most of the previous studies focused on O_3 pollution analysis in megacities (e.g., Beijing and Hong Kong) and coastal cities (e.g., Xiamen), whereas the impact of emission reduction on O_3 pollution and radical

chemistry in a heavy industrial city still remained unknown.

As a typical heavy industrial city in NCP, Tangshan possessed many energy-intensive industries including coal-fired power plants, non-ferrous smelting industries, and cement factories. According to previous estimates, the anthropogenic VOC emissions in Tangshan reached about 2.35 $\times 10^5$ t yr^{-1} (Zhou et al., 2014). Li et al. (2019) further estimated OFP of these released VOCs and found the total OFP in Tangshan (> 150 Gg-O_3/grid) in 2017 was significantly higher than those in most cities over China. It is a typical region to reveal O_3 formation mechanisms and radical chemistry because it could reflect the overall characteristics of NCP. Major aims of this study are to clarify (1) the VOCs and O_3 pollution characteristics after COVID-19 lockdown; (2) the impact of meteorological condition on O_3 increase; (3) AOC and radical chemistry during pandemic period; and (4) the O_3 formation mechanisms and sensitivity. The results are expected to offer scientific evidence for formulating refined ozone management policy in NCP.

2. Materials and methods

2.1 Field measurement

The field campaign about the observation of hourly meteorological factors, VOCs, O_3, and other gaseous pollutants was performed at a supersite in Tangshan during 1 January-7 February, 2020 (Figure S1). The sampling site was located in the center of urban, Tangshan. It is surrounded by residential and commercial areas. Some energy-intensive industries were around 50 kilometers away from this supersite. The meteorological factors including air temperature (T), P, RH, WS, and wind direction (WD) were measured by a weather station with a sonic anemometer (150WX, Airmar, USA). O_3, SO_2, NO_2, and CO levels were measured by commercial trace gas analyzer TEI 49i, 43i, 42i, and 48i (Thermo Fisher Scientific, USA), respectively. The HONO concentration was measured by Monitoring Aerosols and Gases in Ambient Air (MARGA; ADI 2080). A gas chromatography-mass spectrometer (GC-FID/MS) was applied to monitor at least 50 species of VOC concentrations with a 1 h time resolution (Table S1). The quality assurance of O_3, SO_2, NO_2, and CO was performed based on HJ 630-2011 specifications. The limits of detection (LODs), precisions and accuracies of the VOC analyses were 4-9 ppt, 2%, and 5%, respectively. All of these techniques have been widely used in previous studies, and some detailed descriptions have been documented in our companion paper (Li et al., 2021).

2.2 Model development

The ambient O_3 concentration was affected by the comprehensive impacts of meteorological conditions and emissions. In order to distinguish the separate contributions of emission and meteorology, a random forest (RF) approach was utilized to serve as the site-specific modeling platform (Chen et al., 2018). The hourly O_3 level was regarded as the dependent variables, while the meteorological factors including T, P, RH, WS, and WD, and time predictors (year, day of year (DOY), day of week (DOW), hour) served as the independent variables. The 10-fold cross-validation algorithm was applied to examine the performance of this approach. The original dataset was randomly classified into a training dataset (90% of the original dataset) for developing the RF model and the remained 10% was regarded as the test dataset. After the establishment of the RF model, the deweathered algorithm was used to estimate the O_3 level at a specific time point (e.g., 2020/02/05 16:00). The difference of observed O_3 level and deweathered O_3 level was treated as the concentrations contributed by meteorology. Some typical statistical indexes such as R^2 value, RMSE, and MAE could be treated as the major criteria to evaluate the modelling performance. In general, the RF model with the R^2 value higher than 0.50 was considered to be the reliable result. In our study, some hyperparameters such as the number of trees (ntree), number of samples (nsample) and the minimal node size in RF model was set as 500, 500, and 5, respectively.

2.3 GAM model

The RF model cannot assess the isolated impact of each meteorological parameter on ambient O3 concentration. Therefore, the GAM model was further applied to quantify the isolated effect. The detailed algorithm of the GAM model was as follows:

$$g(\mu) = a + \sum f_i(X_i) \qquad (1)$$

where $\mu=E(Y|X_1,X_2\ldots\ldots X_m)$; $g(\mu)$ represents the contiguous function; fp is the smooth function; Xp denotes the independent variables.

2.4 GEOS-Chem model

In order to assess the impact of regional transport on O_3 pollution in Tangshan, the GEOS-Chem model (v12-01) driven by GEOS-FP assimilated meteorological data was employed to simulate the ambient O_3 level during 1 January-7 February, 2020. The GEOS-Chem model included detailed ozone-NO_x-VOC-PM-halogen tropospheric chemistry. The nested grid version of the model with a horizontal resolution of 0.25° × 0.3125° was used. The anthropogenic emission

inventory in 2019 was collected from Community Emissions Data System (CEDS) (Hoesly et al., 2018). Then, the emission inventory in 2020 was calculated based on that in 2019 and updated adjustment factor proposed by (Doumbia et al., 2021). Natural emissions include open biomass burning, lightning, and soil release. Open fire emissions from GFED4 in 2019 were used for both of 2019 and 2020 simulations (Van Der Werf et al., 2017). Lightning NO_X emission was constrained by the average of LIS/OTD satellite observations from 1995 to 2013 (Hudman et al., 2012; Murray et al., 2012). The contributions of regional transport to ambient O_3 before and after COVID-19 lockdown could be quantified based on this model.

2.5 Observation-based chemical box model

In our study, OBM coupled with MCM v3.3.1 was applied to investigate the O_3 formation mechanisms and the radical chemistry. More than 6700 chemical species and 17,000 reactions were included in this model. The observation parameters of the gaseous pollutants including O_3, SO_2, CO, HONO, NO, NO_2, and VOCs, and meteorological parameters including T, RH, and P were utilized to constrain the model. In addition, the photolysis frequencies (J values) were also incorporated into the model, which was calculated as a function of solar zenith angle and altitude based on Tropospheric Ultraviolet and Visible (TUV) model. Before each simulation, the model was run for 5 d as spin-up to ensure the stable state and modelling reliability. AOC was estimated based on the following equations:

$$AOC = \sum_{i=1} k_{Y_i - X} Y_i X \qquad (2)$$

where Y_i represents the targeted pollutants (e.g., CH_4, VOCs, and CO), X represents key oxidants (OH, NO_3, and O_3), and $k_{Yi\text{-}X}$ denotes the rate constants for the reactions of Y_i and X.

The production reaction of O_3 includes RO_2+NO and HO_2+NO, while the removal reaction of O_3 involves O_3 photolysis, O_3+HO_2, O_3+OH, NO_2+OH, NO_3+VOCs, and O_3+VOCs. The net O_3 production was equaled to the difference of $P(O_3)$ and $L(O_3)$. The detailed equations are as follows:

$$P(O_3) = k_1[NO][HO_2] + \sum k_{2i}[NO][RO_2] \qquad (3)$$

$$L(O_3) = k_3[O_1D][H_2O] + k_4[O_3][HO_2] + k_5[O_3][OH] + k_6[NO_2][OH] + \sum k_{7i}[O_3][VOCs] \qquad (4)$$

$$N(O_3) = P(O_3) - L(O_3) \qquad (5)$$

where k_i is the related reaction rate constant. $P(O_3)$, $L(O_3)$, and $N(O_3)$ denote the production, loss,

and net production rate of ambient O_3.

In addition, to assess the impact of aerosol uptake on O_3 production, we also added the heterogeneous uptake of HO_2 in the box model when the sensitivity experiment was performed. The impact of heterogeneous reaction of HO_2 on ozone formation was estimated in the box model using RH-corrected aerosol surface concentration (S_a) and uptake coefficient of HO_2. The change rate in HO_2 due to aerosol uptake is expressed by Eq. (6).

$$\frac{dC}{dt} = \frac{\gamma_{HO2} \times v \times S_a \times C}{4} \quad (6)$$

where C, v, and γ_{HO2} represent the gas-phase concentration, mean molecular velocity, and uptake coefficient, respectively. The measured RH to correct S_a to ambient conditions. The uptake coefficient of HO_2 was equaled to 0.2, which has been widely used by previous studies (Wang et al., 2020b; Taketani et al., 2012).

As the quotient of O_3 change ratio and precursor change ratio, RIR is defined to diagnose the O_3 sensitivity to precursors. The detailed equation is as follows:

$$RIR = \frac{\Delta P(O_3) / P(O_3)}{\Delta Y / Y} \quad (7)$$

Where RIR reflects the relative incremental reactivity; Δ denotes the increase rate; Y represents the precursor of O_3 formation.

The index of agreement (IOA) was defined as an index to evaluate the modelling performance of OBM-MCM. In general, the result could be considered to be robust when the IOA value was higher than 0.7. The IOA in our study reached 0.8. Thus, the performance of the OBM-MCM was acceptable. The detailed algorithm of IOA was introduced in Liu et al. (2019) and Liu et al. (2022).

3. Results and discussion

3.1 Overview of observations

The temporal variations of meteorological parameters are depicted in Figure 1. During the whole observation period, the prevailing WD was northwestly. The hourly average T remained stable characteristic, while RH, P, and WS increased from 58%, 1019 hPa, and 0.9 m/s to 60%, 1023 hPa, and 1.3 m/s after COVID-19 lockdown, respectively (Table S2). Compared with the pre-lockdown period, the concentrations of SO_2, CO, NO, NO_2, and total VOCs (TVOCs) decreased by 0.9%, 2.5%, 85%, 41%, and 42% during COVID-19 period, respectively. However, the O_3

concentration increased by 143% after COVID-19 lockdown. Nearly all of the gaseous pollutants except O_3 displayed decreasing trend after COVID-19 lockdown. It was assumed that many strict lockdown measures such as partial or complete closure of international borders and nonessential businesses, and restricted citizen mobility largely reduced the precursor emissions (Goldberg et al., 2020; Venter et al., 2020). Besides, the increased RH and WS were beneficial to the secondary transformation from NO_x to NO_3^-, and the diffusion and advection of NO_x, respectively (Huang et al., 2021; Li et al., 2021b). Both of these meteorological conditions promoted the decrease of ambient NO_x concentration. Compared with NO_x and TVOCs, SO_2 and CO levels suffered from slight decreases. It was supposed that home order largely increased the residential emission (Doumbia et al., 2021; Saha et al., 2022; Zheng et al., 2020), which might offset the decreases of vehicle and industrial emissions. There are many reasons accounting for the substantial increase of ambient O_3 concentration. Based on the rough analysis, the ratio of VOC/NO_x during the business-as-usual period was around 0.7, which could be defined as the VOC-limited region (Li et al., 2021a). After COVID-19 lockdown period, the decreasing trend of NO_x (59%) was much higher than that of TVOCs (41), which aggravated the rebound of O_3 concentration. In addition, the increased P might exacerbate O_3 pollution though T remained stable during COVID-19 period (Chen et al., 2019; Dong et al., 2020; Wang et al., 2022).

The analysis of TVOC variation alone cannot reveal the O_3 increase after COVID-19 lockdown, the detailed variations of VOC species was necessary. During the whole observation period, alkanes dominated the TVOC concentration with the hourly average concentration of 35±11 ppbv. Following alkanes, the alkenes and OVOCs accounted for 20% and 13% of TVOC concentrations, respectively (Figure 2 and S2). Compared with the business-as-usual period, the concentrations of alkanes, alkenes, aromatics, OVOCs, and other VOC species decreased by 45%, 28%, 50%, 41%, and 48% after COVID-19 lockdown, respectively. The most significant drop was found in aromatics, which was similar to the result of Changzhou (Jensen et al., 2021). It might be associated with the drastic decreases in industrial activities and traffic volumes, which were major sources of ambient aromatics. As the key indicators of vehicular exhaust and industrial emission (Song et al., 2020; Zhang et al., 2016), the concentrations of toluene and benzene decreased by 63% and 69%, respectively. The result also demonstrated that the substantial decreases of traffic and industrial emissions were responsible for the significant aromatic decreases. However, the contribution ratios

of VOC species suffered from different variation characteristics. The contribution ratio of alkanes, alkenes, aromatics, OVOCs, and other VOC species accounting for TVOC concentrations changed from 55%, 19%, 4.6%, 13%, and 8.2% to 53%, 23%, 3.9%, 13%, and 7.3%, respectively. The result of the increase of alkenes ratio and the decrease of aromatics ratio was in good agreement with that in Nanjing (Wang et al., 2021). The increase of fraction of alkenes to TVOCs after COVID-19 lockdown might be linked with the emission source. It was well known that the alkenes might be derived from gasoline evaporation and petrochemical industries (Wang et al., 2021; Wang et al., 2020a). Some necessary petrochemical industries were not closed during the pandemic, which caused the slight decreases of alkenes concentrations.

3.2 The impact of meteorology on ambient O_3

3.2.1 The isolated contribution of meteorology and emission to ambient O_3

Deweathered O_3 concentration was estimated based on RF model after the normalization of meteorological parameters. The difference of observed O_3 level and normalized O_3 level represented the O_3 concentration contributed by meteorology. As shown in Figure 3, the observed and normalized O_3 concentrations increased from 8.9 ± 2.2 and 12 ± 2.7 ppb to 22 ± 5.3 and 21 ± 5.1 ppb after COVID-19 lockdown, respectively. The ambient O_3 level increased by 143% during COVID-19 period, and the emission reduction and meteorology contributed to 77% and 66% of this increment, respectively. The result suggested that the excessive NO_x emission reduction and the increase of VOC/NO_x ratio in the VOC-limited region might be the major factors for the substantial increase of ambient O_3 level during the pandemic. In addition, the unfavorable meteorological conditions especially the increase of P and WS aggravated the O_3 pollution (Dong et al., 2020; Ning et al., 2020; Shu et al., 2020).

3.2.2 The effect of each meteorological parameter on O_3 pollution

Although the machine-learning model can quantify the overall contribution of meteorological conditions to O_3 pollution, the impact of each meteorological parameter on ambient O_3 level still remained unknown. Therefore, the generalized additive model (GAM) was employed to capture the complex nonlinear relationships between O_3 and its influencing factors. All of these explanatory variables including T, RH, P, and WS exerted significant nonlinear impacts on O_3 level at the level of $p < 0.01$ and degrees of freedom > 1, indicating that each factor displayed statistical significance. The F values could reflect the importance of these variables, and these explanatory variables

followed the order of WS (32) > T (25) > RH (16) > P (3.6). As depicted in Figure S3, T and RH showed positive and negative correlations with O_3 concentrations, respectively. The result was in good agreement with Liu et al. (2022). Atmospheric O_3 generally showed the higher concentrations when P was higher than 1025 hPa or lower than 1018 hPa. Among all of these meteorological parameters, WS showed the highest variable importance, and the higher WS was favorable for O_3 regional transport. The GEOS-Chem modelling result also suggested that the average O_3 flux induced by regional transport after COVID-19 lockdown reached 31 kg/s, while the mean O_3 flux before pandemic only reached -5.6 kg/s. The contribution from regional transport changed from negative effect to positive effect after COVID-19 lockdown, which largely increased O_3 level during this period. Overall, the combined effects of regional transport and local photochemical production might be responsible for the O_3 increase.

3.3 Chemistry perspective

3.3.1 OFP variations of VOC species after COVID-19 lockdown

The VOC species showed distinct reactivities, and thus the OFP value was applied to assess the contribution of active VOCs to ambient O_3 formation. The OFP value equals to the concentration of each VOC species multiplying the ozone formation potential coefficient (MIR). It should be noted that the OFP value did not represent the absolute concentration of ambient O_3, it only reflected the potential O_3 from the VOC degradation. The temporal variations of VOC species are depicted in Figure 4. The total OFP value decreased from 77±38 to 50±27 ppb after COVID-19 lockdown, indicating marked decreases of VOC reactivities due to drastic lockdown measures. Among all of VOC species, the OFP of aromatics (63%) experienced the most dramatic decrease owing to the decline of vehicle and industrial emissions (Doumbia et al., 2021). However, the OFP values of alkenes and OVOCs only suffered from 31% and 34% decreases during the pandemic, respectively. Therefore, the contribution ratios of alkenes and OVOCs to total OFP increased from 56% and 24% during pre-lockdown period to 60% and 24% after COVID-19 lockdown, respectively. At first, alkenes and OVOCs were mainly generated from gasoline evaporation and secondary formation, respectively (Louie et al., 2013; Maji et al., 2020). Both of these VOC species were not sensitive to lockdown measures compared with alkanes and aromatics, both of which were mainly sourced from vehicle emission (Harrison et al., 2021; Mozaffar and Zhang, 2020). Furthermore, the secondary formation could largely compensate for the decrease in primary emissions of OVOCs (Huang et al.,

2019). Moreover, the enhanced regional transport coupled with increased AOC was also beneficial to the secondary formation of OVOCs (Huang et al., 2020; Wu et al., 2020).

Overall, it should be noted that the VOC/NO_x ratio increased from 0.7 to 1.1 after COVID-19 lockdown because the NO_x emission suffered from more dramatic decrease during the pandemic. Meanwhile, the ambient O_3 level also exhibited remarkable increase during the same period. The result suggested that the control of VOCs rather than NO_x might be more effective in reducing ozone level in Tangshan. We further analyzed the contributions of various VOC species to O_3 level, and found the increases in the contributions of alkenes and OVOCs to TVOCs largely elevated ambient O_3 level. Therefore, the effective control of alkenes and OVOCs emissions facilitated the O_3 pollution alleviation.

3.3.2 AOC and radical chemistry after COVID-19 lockdown

In order to further explain the reason for O_3 increase, two cases including pre-lockdown and lockdown periods were selected to analyze the detailed formation/removal mechanisms of O_3 and radicals The IOA value of MCM reached 0.8, indicating the modelling performance was reliable (Chen et al., 2020). The simulated daytime OH concentration displayed a remarkable increase from $(0.6\pm0.4)\times10^6$ to $(1.5\pm1.0)\times10^6$ molecules cm^{-3}. It might be associated with the solar radiation. Moreover, abundant primary pollutants might react with OH during business-as-usual period, which decreased the OH level. Meanwhile, we also estimated daytime AOC before and after COVID-19 lockdown. The result suggested that average daytime AOC increased from 1.0×10^7 molecules cm^{-3} s^{-1} to 1.3×10^7 molecules cm^{-3} s^{-1}. The daytime AOC in the winter of Tangshan was significantly lower than that in autumn of Xiamen (6.7×10^7) and summer of Hong Kong (6.2×10^7) (Liu et al., 2022; Xue et al., 2016). It was supposed that the solar radiation in winter was much lower than that in summer and autumn (Jin et al., 2005; Tang et al., 2010). However, AOC in our study was significantly higher than that during the same period in Changzhou (Zhang et al., 2022a). As shown in Figure 5, the contribution of OH to AOC reached 85% during the whole study period, and thus the higher OH concentration in Tangshan was responsible for the higher AOC compared with Changzhou.

Besides, we further analyzed the reason for OH increase after COVID-19 lockdown from the perspective of budget. OH radical was mainly generated from the reaction of HO_2 + NO, accounting for 61±10% and 76±15% of the total production during pre-lockdown and lockdown periods,

respectively (Figure 6). Following the reaction of HO_2+NO, the processes of HONO photolysis accounted for 36±9% and 22±7% of the total OH production during two cases, respectively. Other pathways including O(1D) + H_2O, O_3 + VOCs, and H_2O_2 photolysis only accounted minor contribution (< 5%) to OH formation. From the perspective of temporal variation, the formation rate from HO_2 + NO increased from 0.7×10^7 during pre-lockdown period to 1.6×10^7 molecules cm^{-3} s^{-1} during the pandemic. However, other formation pathways remained relatively stable characteristics after COVID-19 lockdown. The result indicated that HO_2 + NO was considered to be the major pathway for the significant increase of OH level during the pandemic.

Apart from the analysis of OH formation process, the change of OH loss pathway could also play an important role on the OH increase. It was well documented that OH was mainly depleted by four reactions with CO, VOCs, NO, and NO_2. All of the loss reactions of OH during pre-lockdown period were in the order of OH + NO (34±9%) > OH + NO_2 (23±7%) = OH + VOCs (23±6%) > OH + CO (20±5%), while the loss pathways of OH after COVID-19 lockdown followed the order of OH + VOCs (43±11%) = OH + NO_2 (22±8%) > OH + CO (18±6%) > OH + NO (17±3%). It should be noted that the contribution of NO to OH loss experienced dramatic decrease after COVID-19 lockdown because the strict lockdown measures largely decreased NO emission, which could be treated as a nonnegligible reason for the OH increase during the pandemic. Besides, we also found that the contribution ratio of OH + VOCs showed slight increase because the decreasing ratios of VOC species were relatively lower than those of NO_x.

3.3.3 The chemical mechanisms for O_3 increase after COVID-19 lockdown and implications

The formation and loss pathways of O_3 were depicted in Figure 7. The formation of ambient O_3 was dominated by RO_2 + NO and HO_2 + NO. In our study, the daytime rate of HO_2 + NO during pre-lockdown period reached 2.3 ± 1.1 ppb h^{-1}, accounting for 61% of the total O_3 production. The result was consistent with many previous studies because OH radical was the initiator of O_3 photochemical production. Following the pathway of HO_2 + NO, RO_2 + NO (1.5 ± 0.6 ppb h^{-1}) was also an important pathway for the O_3 formation, accounting for 39% of the total O_3 production. After COVID-19 lockdown, the daytime rates of HO_2+NO and RO_2+NO exhibited significant increases by 61% and 53%, respectively. The loss rates of ambient O_3 during pre-lockdown and lockdown periods showed similar characteristics and they followed the order of NO_2 + OH (59% and 42%) > O_3 photolysis (27% and 33%) > RO_2 + NO_2 (12% and 23%), whereas other pathways

such as O_3 + OH, O_3 + HO_2, O_3 + VOCs, and NO_3 + VOCs contributed limitedly. Although both of $P(O_3)$ and $L(O_3)$ displayed increases after COVID-19 lockdown, the increase of total O_3 production was much higher than that of O_3 loss. Thus, the net production rate of O_3 increased from 2.8 ± 1.3 to 4.6 ± 1.7 ppb h^{-1} after COVID-19 lockdown, which fully explained the rapid increase of ambient O_3 level during the pandemic. Compared with the previous studies, the net production rate of O_3 was much lower than those in summer or autumn of Xiamen (9.1 ± 5.7 ppb h^{-1}) and Shanghai (26 ppb h^{-1}), while it was slightly higher than that in winter of Shanghai (~4 ppb h^{-1}). The difference was strongly dependent on the precursor emissions and photochemical conditions of O_3 formation.

Apart from more rapid decrease of NO_x level compared with VOCs, the excessive reduction of $PM_{2.5}$ concentration after COVID-19 lockdown cannot be ignored because aerosol particles generally scavenged HO_2 radicals (Shi and Brasseur, 2020). As shown in Figure 7, the daytime O_3 production rates from HO_2+NO accounted for the major fraction of all of the pathways before and after COVID-19 lockdown, and the HO_2 radical level displayed drastic increase (61%) after lockdown. To evaluate the impact of aerosol variation on HO_2 radical, the aerosol uptake of HO_2 radical was added into the model and its impact on the contribution of HO_2+NO on O_3 production were compared with that without aerosol module (Figure S4). The result suggested that the daytime O_3 production rate derived from HO_2+NO without aerosol module only increased by 61% after lockdown, while the daytime O_3 formation rate from HO_2+NO pathway with aerosol uptake increased by 80% (Figure S4). The result indicated that the rapid reduction of aerosol surface area after lockdown weakened the HO_2 uptake, and thus aggravated the O_3 production derived from HO_2+NO pathway. The result was in good agreement with some previous studies (Wang et al., 2020b; Tan et al., 2022).

To examine the impacts of precursor emissions (various VOC species) on O_3 production, RIR technique was applied to diagnose the O_3 sensitivity to precursors (Figure 8). First of all, all of the VOCs were classified into anthropogenic hydrocarbons (AHCs) and biogenic hydrocarbons (BHCs) (e.g., isoprene). Afterwards, all of AHCs could be further categorized into four groups of alkanes, alkenes, aromatics, and OVOCs. The O_3 production was highly VOC-sensitive especially AHCs-sensitive (RIR: 0.8), followed by CO (0.2), and BHCs (0.1). However, the NO_x showed the negative impact on O_3 production in Tangshan (RIR: -0.59). Among all of the AHCs, the contributions to O_3 sensitivity were in the order of alkenes (0.4) > OVOCs (0.3) > alkanes (0.1) ≥ aromatics (0.1).

Although the RIR value has revealed the importance of VOCs and NO_x on O_3 formation, this method cannot quantify the contribution of VOC species and NO_x to ambient O_3 change. Therefore, the scenario analysis raised a question: how much O_3 could change with the reduction of VOC species and NO_x? Then, the variation percentage of ambient O_3 was calculated, which was beneficial to the implementation of O_3 control strategies. As shown in Figure 9a, nearly all of the VOC species displayed the positive relationships with O_3 variations. Similar to RIR values, O_3 level suffered from the most significant response to alkenes. In our study, the O_3 production experienced around 30% decrease when the alkenes decreased by 80%. Following alkenes, the O_3 reduction reached 25%, 10%, and 12% when OVOCs, alkanes, and aromatics decreased by 80%, respectively. The results also confirmed that the decreases of alkenes and OVOCs could alleviate O_3 pollution effectively. As depicted in Figure 9b, the NO_x level exhibited negative correlation with O_3 production. The O_3 production could increase by 50% when NO_x experienced 80% reduction. Although Tangshan has experienced rapid NO_x decrease in the past years and the NO_2 concentration in Tangshan remained the lower level, Tangshan was still VOC-limited regime. The continuous NO_x reduction might be not an efficient pathway for O_3 pollution control.

Although many previous studies have confirmed more rapid NO_x reduction compared with VOCs might be responsible for the O_3 increase, the comprehensive impacts of each VOC species and NO_x on ambient O_3 and their interactions with meteorology were not revealed clearly. Based on the detailed analysis in our study, collaborative controls VOC and NO_x must be seriously performed in the near future. Moreover, more efforts are needed for the control of alkenes and OVOCs. Li et al. (2019) revealed the emissions of alkenes and OVOCs derived from paint use and chemical industry across China experienced rapid increases since 2010 and will keep the trend in the near future. Therefore, our policy implication will benefit not just NCP but also other regions in China.

4. Conclusions

Due to the outbreak of COVID-19, many strict lockdown measures have been widely adopted across China, leading to dramatic decreases of vehicle and industrial emissions. Therefore, the concentrations of multiple air pollutants such as SO_2, NO_x, and CO experienced decreases during the pandemic, whereas the O_3 level suffered from significant increase. To uncover the reason for O_3 increase, the precursor concentrations (e.g., VOCs, NO_x), meteorological conditions, and relevant chemical mechanisms have been analyzed. The ambient O_3 level increased by 143% during COVID-

19 period, and the emission reduction and meteorology contributed to 77% and 66% of this increment, respectively. Along with the obvious increase of O_3 concentration, the VOC/NO_x ratio also increased from 0.7 to 1.1 after COVID-19 lockdown, indicating the control of VOCs rather than NO_x might be more effective in reducing O_3 level in Tangshan. In addition, the OFP values of VOC species were also calculated to assess their contributions to O_3 formation. We found that the alkenes and OVOCs displayed the higher contributions to O_3 production. Afterwards, a box model was applied to further analyze the detailed chemical mechanisms of O_3 formation and sensitivity. The result suggested that increased contributions of HO_2+NO and RO_2+NO resulted in the significant increase of O_3 concentration. Besides, the O_3 sensitivity analysis also demonstrated that the alkenes and OVOCs played significant roles on the O_3 formation and the reduction of alkenes and OVOCs were more beneficial to O_3 mitigation. In regard with the temporal trends of VOC emissions over China, more efforts should be devoted to reduce the concentrations of alkenes and OVOCs across China rather than NCP alone.

Acknowledgements

This work was supported by the National Natural Science Foundation of China (42107113).

Data availability

[Dataset] The CEDS emission inventory are available at the website of https://zenodo.org/record/3754964#.YwrJL8jfmfU (McDuffie et al., 2020).

Author contributions

LR wrote the manuscript. LR and WGH contributed to the conceptualization of the study. GYN, and LR conducted the research, and visualized the results. LR and GYN revised the manuscript.

Competing interests

The contact author has declared that neither they nor their co-authors have any competing interests.

References

Chen, T., Xue, L., Zheng, P., Zhang, Y., Liu, Y., Sun, J., Han, G., Li, H., Zhang, X., Li, Y. (2020) Volatile organic compounds and ozone air pollution in an oil production region in northern China. Atmospheric Chemistry and Physics 20, 7069-7086.

Chen, Z., Zhuang, Y., Xie, X., Chen, D., Cheng, N., Yang, L., Li, R. (2019) Understanding long-term variations of meteorological influences on ground ozone concentrations in Beijing During 2006–2016. Environmental pollution 245, 29-37.

Dong, Y., Li, J., Guo, J., Jiang, Z., Chu, Y., Chang, L., Yang, Y., Liao, H. (2020) The impact of synoptic patterns on summertime ozone pollution in the North China Plain. Science of the Total Environment 735, 139559.

Doumbia, T., Granier, C., Elguindi, N., Bouarar, I., Darras, S., Brasseur, G., Gaubert, B., Liu, Y., Shi, X., Stavrakou, T. (2021) Changes in global air pollutant emissions during the COVID-19 pandemic: a dataset for atmospheric modeling. Earth System Science Data 13, 4191-4206.

Goldberg, D.L., Anenberg, S.C., Griffin, D., McLinden, C.A., Lu, Z., Streets, D.G. (2020) Disentangling the impact of the COVID-19 lockdowns on urban NO2 from natural variability. Geophysical Research Letters 47, e2020GL089269.

Goldberg, D.L., Harkey, M., de Foy, B., Judd, L., Johnson, J., Yarwood, G., Holloway, T. (2022) Evaluating NOx emissions and their effect on O3 production in Texas using TROPOMI NO2 and HCHO. Atmos. Chem. Phys. 22, 10875-10900.

Gong, X., Hong, S., Jaffe, D.A. (2018) Ozone in China: Spatial distribution and leading meteorological factors controlling O3 in 16 Chinese cities. Aerosol and Air Quality Research 18, 2287-2300.

Harrison, R.M., Allan, J., Carruthers, D., Heal, M.R., Lewis, A.C., Marner, B., Murrells, T., Williams, A. (2021) Non-exhaust vehicle emissions of particulate matter and VOC from road traffic: A review. Atmospheric Environment 262, 118592.

Hoesly, R.M., Smith, S.J., Feng, L., Klimont, Z., Janssens-Maenhout, G., Pitkanen, T., Seibert, J.J., Vu, L., Andres, R.J., Bolt, R.M. (2018) Historical (1750–2014) anthropogenic emissions of reactive gases and aerosols from the Community Emissions Data System (CEDS). Geoscientific Model Development 11, 369-408.

Huang, X.-F., Wang, C., Zhu, B., Lin, L.-L., He, L.-Y. (2019) Exploration of sources of OVOCs in various atmospheres in southern China. Environmental pollution 249, 831-842.

Huang, X.-F., Zhang, B., Xia, S.-Y., Han, Y., Wang, C., Yu, G.-H., Feng, N. (2020) Sources of oxygenated volatile organic compounds (OVOCs) in urban atmospheres in North and South China. Environmental pollution 261, 114152.

Huang, X., Ding, A., Gao, J., Zheng, B., Zhou, D., Qi, X., Tang, R., Wang, J., Ren, C., Nie, W. (2021) Enhanced secondary pollution offset reduction of primary emissions during COVID-19 lockdown in China. National Science Review 8, nwaa137.

Hudman, R., Moore, N., Mebust, A., Martin, R., Russell, A., Valin, L., Cohen, R. (2012) Steps towards a mechanistic model of global soil nitric oxide emissions: implementation and space based-constraints. Atmospheric Chemistry and Physics 12, 7779-7795.

Jensen, A., Liu, Z., Tan, W., Dix, B., Chen, T., Koss, A., Zhu, L., Li, L., de Gouw, J. (2021) Measurements of volatile organic compounds during the COVID-19 lockdown in Changzhou, China. Geophysical Research Letters 48, e2021GL095560.

Jin, Z., Yezheng, W., Gang, Y. (2005) General formula for estimation of monthly average daily global solar radiation in China. Energy Conversion and Management 46, 257-268.

Li, M., Zhang, Q., Zheng, B., Tong, D., Lei, Y., Liu, F., Hong, C., Kang, S., Yan, L., Zhang, Y. (2019) Persistent growth of anthropogenic non-methane volatile organic compound (NMVOC) emissions in China during 1990-2017: drivers, speciation and ozone formation potential. Atmospheric Chemistry and Physics 19, 8897-8913.

Li, R., Xu, M., Li, M., Chen, Z., Zhao, N., Gao, B., Yao, Q. (2021a) Identifying the spatiotemporal variations in ozone formation regimes across China from 2005 to 2019 based on polynomial simulation and causality analysis. Atmospheric Chemistry and Physics 21, 15631-15646.

Li, R., Zhao, Y., Fu, H., Chen, J., Peng, M., Wang, C. (2021b) Substantial changes in gaseous pollutants and chemical compositions in fine particles in the North China Plain during the COVID-19 lockdown period: anthropogenic vs. meteorological influences. Atmospheric Chemistry and Physics 21, 8677-8692.

Li, X., Qin, M., Li, L., Gong, K., Shen, H., Li, J., Hu, J. (2022) Examining the implications of photochemical indicators on the O3-NOx-VOC sensitivity and control strategies: A case study in the Yangtze River Delta (YRD), China. Atmos. Chem. Phys. Discuss. 2022, 1-24.

Liu, T., Hong, Y., Li, M., Xu, L., Chen, J., Bian, Y., Yang, C., Dan, Y., Zhang, Y., Xue, L. (2022) Atmospheric oxidation capacity and ozone pollution mechanism in a coastal city of southeastern China: analysis of a typical photochemical episode by an observation-based model. Atmospheric Chemistry and Physics 22, 2173-2190.

Liu, X., Lyu, X., Wang, Y., Jiang, F., Guo, H. (2019) Intercomparison of O 3 formation and radical chemistry in the past decade at a suburban site in Hong Kong. Atmospheric Chemistry and Physics 19, 5127-5145.

Louie, P.K., Ho, J.W., Tsang, R.C., Blake, D.R., Lau, A.K., Yu, J.Z., Yuan, Z., Wang, X., Shao, M., Zhong, L. (2013) VOCs and OVOCs distribution and control policy implications in Pearl River Delta region, China. Atmospheric Environment 76, 125-135.

Maji, S., Beig, G., Yadav, R. (2020) Winter VOCs and OVOCs measured with PTR-MS at an urban site of India: role of emissions, meteorology and photochemical sources. Environmental pollution 258, 113651.

Mozaffar, A., Zhang, Y.-L. (2020) Atmospheric volatile organic compounds (VOCs) in China: a review. Current Pollution Reports 6, 250-263.

McDuffie, E.E., Smith, S.J., Rourke, P.O., Tibrewal, K., Venkataraman, C., Marais, E.A., Zheng, B., Crippa, M., Brauer, M., Martin, R.V. (2020) A global anthropogenic emission inventory of atmospheric pollutants from sector- and fuel-specific sources (1970-2017): an application of the Community Emissions Data System (CEDS) [Dataset]. Earth System Science Data 12, 3413–3442.

Murray, L.T., Jacob, D.J., Logan, J.A., Hudman, R.C., Koshak, W.J. (2012) Optimized regional and interannual variability of lightning in a global chemical transport model constrained by LIS/OTD satellite data. Journal of Geophysical Research: Atmospheres 117.

Ning, G., Yim, S.H.L., Yang, Y., Gu, Y., Dong, G. (2020) Modulations of synoptic and climatic changes on ozone pollution and its health risks in mountain-basin areas. Atmospheric Environment 240, 117808.

Nussbaumer, C.M., Pozzer, A., Tadic, I., Röder, L., Obersteiner, F., Harder, H., Lelieveld, J., Fischer, H. (2022) Tropospheric ozone production and chemical regime analysis during the COVID-19 lockdown over Europe. Atmos. Chem. Phys. 22, 6151-6165.

Saha, L., Kumar, A., Kumar, S., Korstad, J., Srivastava, S., Bauddh, K. (2022) The impact of the COVID-19 lockdown on global air quality: A review. Environmental Sustainability, 1-19.

Shi, X., Brasseur, G.P. (2020) The response in air quality to the reduction of Chinese economic activities

during the COVID-19 outbreak. Geophysical Research Letters 47, e2020GL088070.
Shu, L., Wang, T., Han, H., Xie, M., Chen, P., Li, M., Wu, H. (2020) Summertime ozone pollution in the Yangtze River Delta of eastern China during 2013–2017: Synoptic impacts and source apportionment. Environmental pollution 257, 113631.
Song, C., Liu, Y., Sun, L., Zhang, Q., Mao, H. (2020) Emissions of volatile organic compounds (VOCs) from gasoline-and liquified natural gas (LNG)-fueled vehicles in tunnel studies. Atmospheric Environment 234, 117626.
Taketani, F., Kanaya, Y., and Akimoto, H.: Kinetics of heterogeneous reactions of HO_2 radical at ambient concentration levels with $(NH_4)_2SO_4$ and NaCl aerosol particles, J. Phys. Chem. A, 112, 2370–2377, 2008.
Tan, Z.F., Lu, K.D., Ma, X.F., Chen, S.Y., He, L.Y., Huang, X.F., Li, X., Lin, X.Y., Tang, M.X., Yu, D., Wahner, A., Zhang, Y.H. (2022) Multiple impacts of aerosols on O_3 production are largely compensated: a case study Shenzhen, China. Environ. Sci. Tech. https://doi.org/10.1021/acs.est.2c06217
Tang, W., Yang, K., He, J., Qin, J. (2010) Quality control and estimation of global solar radiation in China. Solar Energy 84, 466-475.
Van Der Werf, G.R., Randerson, J.T., Giglio, L., Van Leeuwen, T.T., Chen, Y., Rogers, B.M., Mu, M., Van Marle, M.J., Morton, D.C., Collatz, G.J. (2017) Global fire emissions estimates during 1997–2016. Earth System Science Data 9, 697-720.
Venter, Z.S., Aunan, K., Chowdhury, S., Lelieveld, J. (2020) COVID-19 lockdowns cause global air pollution declines. Proceedings of the National Academy of Sciences 117, 18984-18990.
Wang, M., Lu, S., Shao, M., Zeng, L., Zheng, J., Xie, F., Lin, H., Hu, K., Lu, X. (2021) Impact of COVID-19 lockdown on ambient levels and sources of volatile organic compounds (VOCs) in Nanjing, China. Science of the Total Environment 757, 143823.
Wang, M., Qin, W., Chen, W., Zhang, L., Zhang, Y., Zhang, X., Xie, X. (2020a) Seasonal variability of VOCs in Nanjing, Yangtze River delta: Implications for emission sources and photochemistry. Atmospheric Environment 223, 117254.
Wang, W.J., Parrish, D., Li, X., Shao, M., Liu, Y., Mo, Z.W., Lu, S.H., Hu, M., Fang, X., Wu, Y.S., Zeng, L.M., Zhang, Y.H. (2020b) Exploring the drivers of the increased ozone production in Beijing in summertime during 2005–2016. Atmos. Chem. Phys. 20, 15617–15633.
Wang, P., Yang, Y., Li, H., Chen, L., Dang, R., Xue, D., Li, B., Tang, J., Leung, L.R., Liao, H. (2022) North China Plain as a hot spot of ozone pollution exacerbated by extreme high temperatures. Atmospheric Chemistry and Physics 22, 4705-4719.
Wang, Y., Wen, Y., Wang, Y., Zhang, S., Zhang, K.M., Zheng, H., Xing, J., Wu, Y., Hao, J. (2020b) Four-month changes in air quality during and after the COVID-19 lockdown in six megacities in China. Environmental Science & Technology Letters 7, 802-808.
Wu, C., Wang, C., Wang, S., Wang, W., Yuan, B., Qi, J., Wang, B., Wang, H., Wang, C., Song, W. (2020) Measurement report: Important contributions of oxygenated compounds to emissions and chemistry of volatile organic compounds in urban air. Atmospheric Chemistry and Physics 20, 14769-14785.
Xue, L., Gu, R., Wang, T., Wang, X., Saunders, S., Blake, D., Louie, P.K., Luk, C.W., Simpson, I., Xu, Z. (2016) Oxidative capacity and radical chemistry in the polluted atmosphere of Hong Kong and Pearl River Delta region: analysis of a severe photochemical smog episode. Atmospheric Chemistry and Physics 16, 9891-9903.
Yin, Z., Wan, Y., Wang, H. (2021) Decadal changes of connections among late-spring snow cover in West

Siberia, summer Eurasia teleconnection and O3-related meteorology in North China. Atmos. Chem. Phys. 21, 11519-11530.

Zhang, K., Liu, Z., Zhang, X., Li, Q., Jensen, A., Tan, W., Huang, L., Wang, Y., de Gouw, J., Li, L. (2022a) Insights into the significant increase in ozone during COVID-19 in a typical urban city of China. Atmospheric Chemistry and Physics 22, 4853-4866.

Zhang, X., Yin, Y., van der A, R., Eskes, H., van Geffen, J., Li, Y., Kuang, X., Lapierre, J.L., Chen, K., Zhen, Z., Hu, J., He, C., Chen, J., Shi, R., Zhang, J., Ye, X., Chen, H. (2022b) Influence of convection on the upper-tropospheric O3 and NOx budget in southeastern China. Atmos. Chem. Phys. 22, 5925-5942.

Zhang, Z., Zhang, Y., Wang, X., Lü, S., Huang, Z., Huang, X., Yang, W., Wang, Y., Zhang, Q. (2016) Spatiotemporal patterns and source implications of aromatic hydrocarbons at six rural sites across China's developed coastal regions. Journal of Geophysical Research: Atmospheres 121, 6669-6687.

Zhao, Y., Zhang, K., Xu, X., Shen, H., Zhu, X., Zhang, Y., Hu, Y., Shen, G. (2020) Substantial changes in nitrogen dioxide and ozone after excluding meteorological impacts during the COVID-19 outbreak in mainland China. Environmental Science & Technology Letters 7, 402-408.

Zheng, B., Zhang, Q., Geng, G., Shi, Q., Lei, Y., He, K. (2020) Changes in China’s anthropogenic emissions during the COVID-19 pandemic. Earth System Science Data Discussions 10.

Zhou, Y., Cheng, S., Chen, D., Lang, J., Zhao, B., Wei, W. (2014) A new statistical approach for establishing high-resolution emission inventory of primary gaseous air pollutants. Atmospheric Environment 94, 392-401.

Figure 1 Temporal variations of meteorological parameters (e.g., T, RH, P) and gaseous pollutants (e.g., SO_2, O_3) during the whole observation. The date is shown in the format month/day/year.

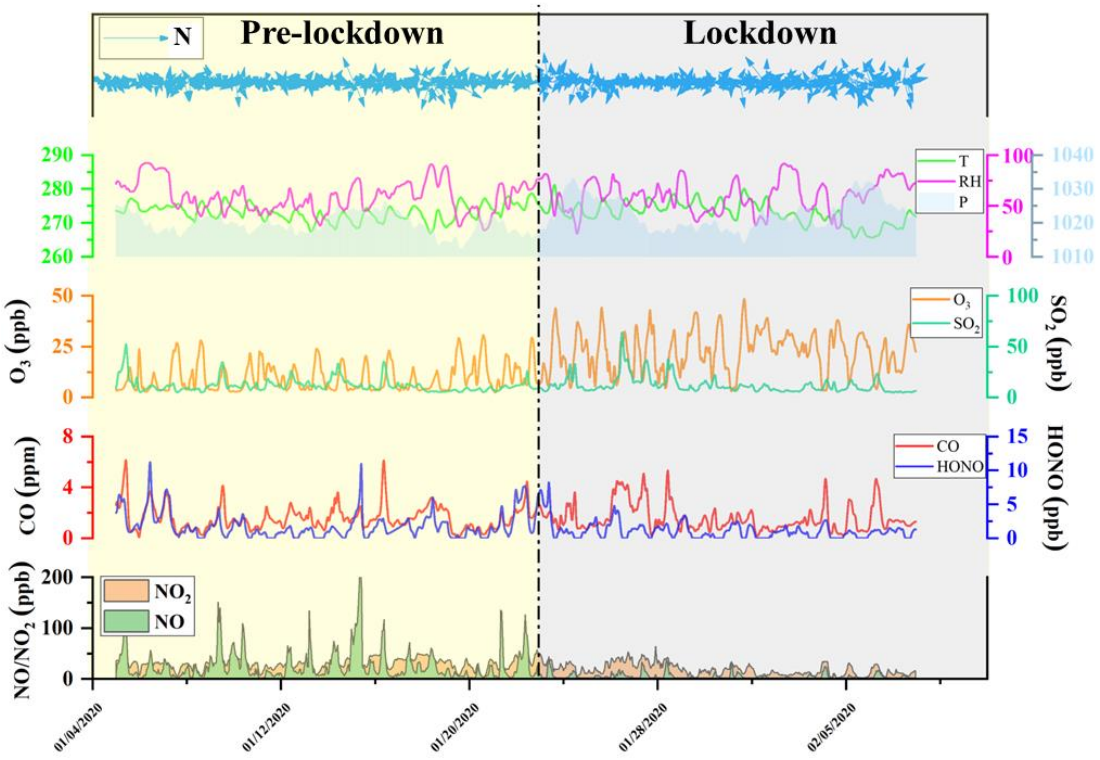

Figure 2 The OFP contribution ratios of VOC species (a). The absolute concentrations (b) and OFP values (c) during pre-lockdown and lockdown periods.

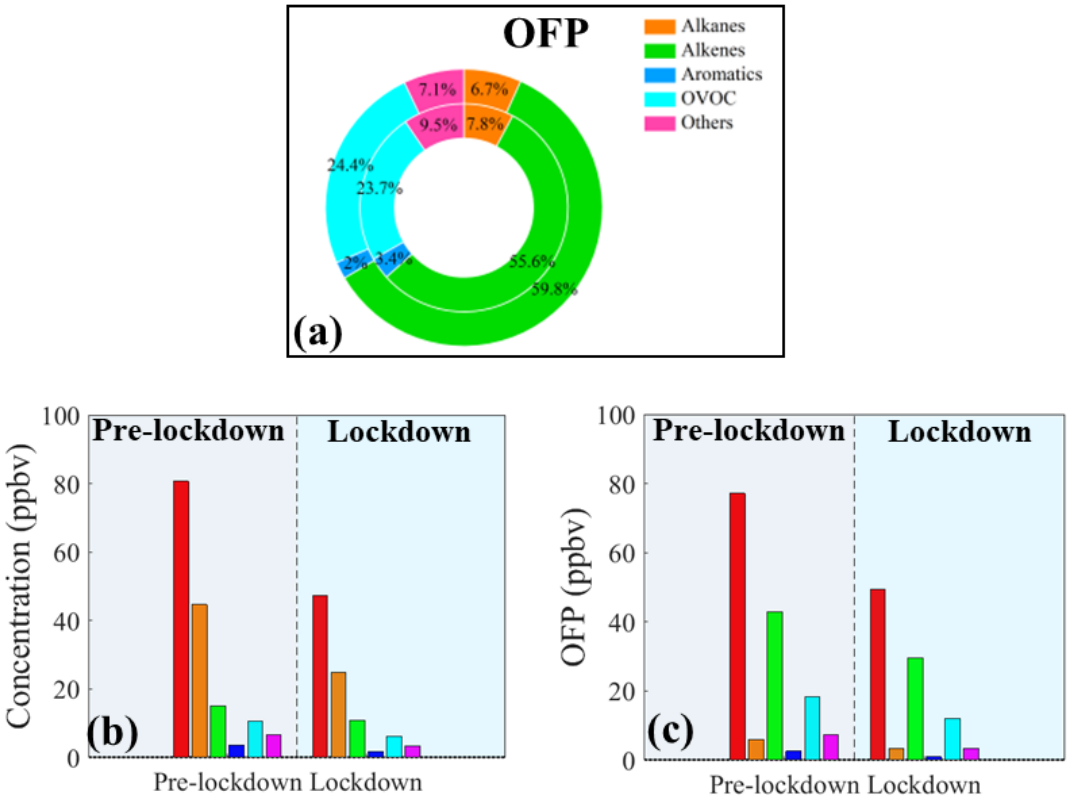

Figure 3 Comparison of observed O_3 (green) and normalized O_3 concentrations (orange) during pre-lockdown and lockdown periods (a). The O_3 change ratios derived from observation, emission, and meteorology.

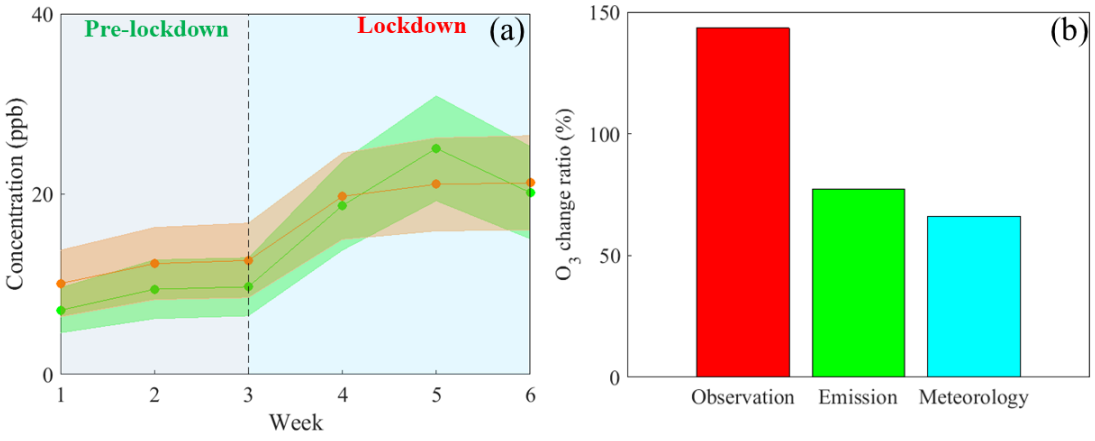

Figure 4 The temporal variations of absolute concentrations (a) and OFP (b) for VOC species during the whole sampling period. The yellow and white episodes represent the pre-lockdown and lockdown periods.

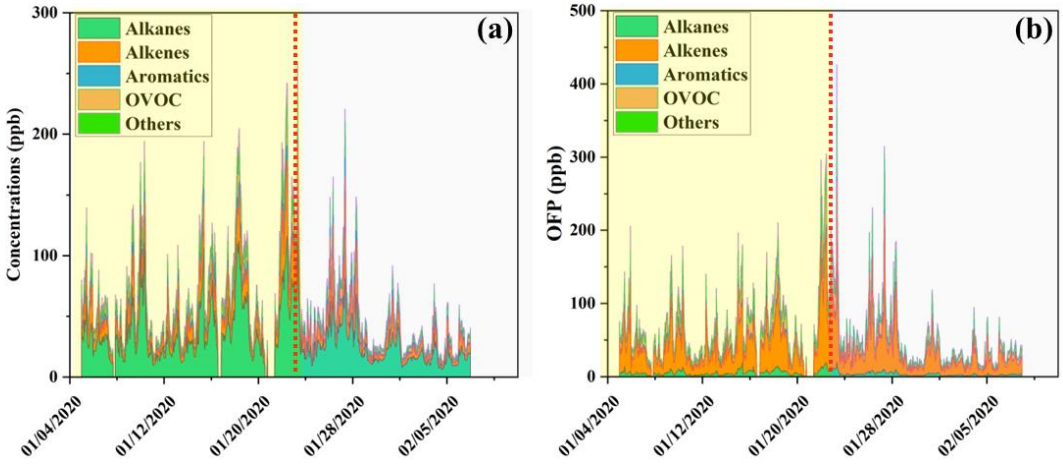

Figure 5 Hourly variations of model-estimated AOC contributed by O_3, OH, and NO_3 radical during pre-lockdown and lockdown periods (Unit: molecules cm^{-3}).

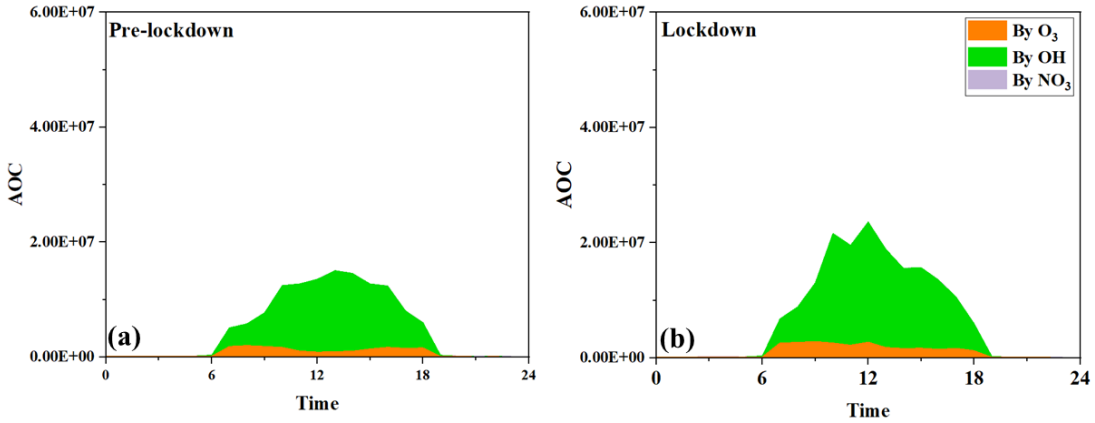

Figure 6 Daytime variation of OH budget during pre-lockdown and lockdown periods.

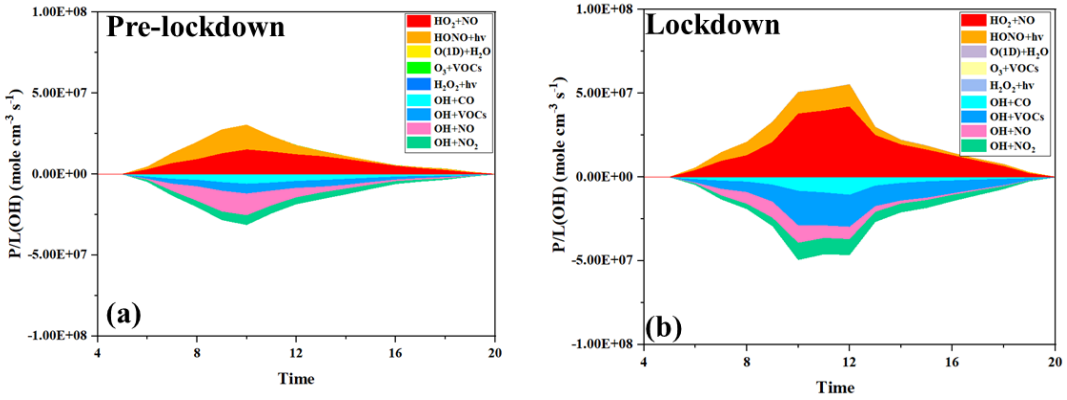

Figure 7 Daytime variation of O_3 budget during pre-lockdown and lockdown periods.

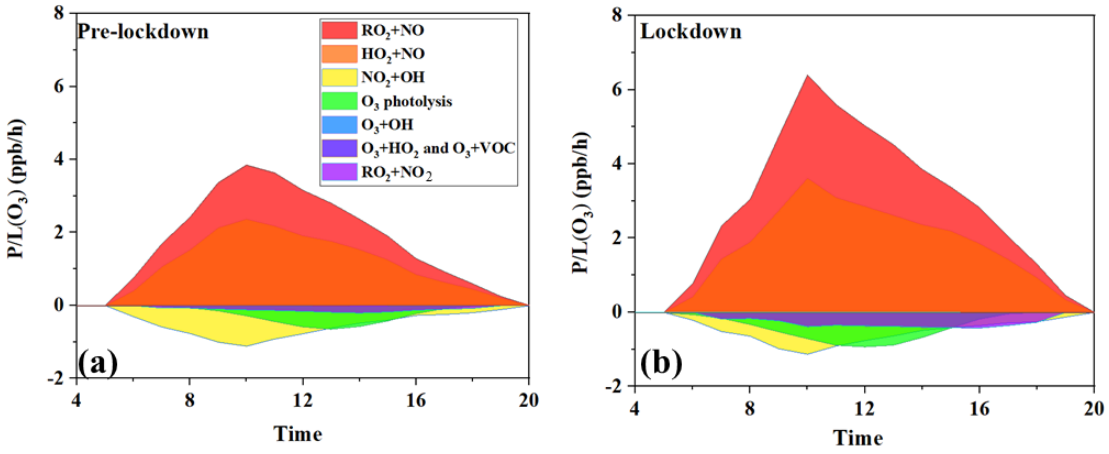

Figure 8 The model-estimated RIR values for major O_3 precursor groups and (b) the sub-groups of anthropogenic VOC species.

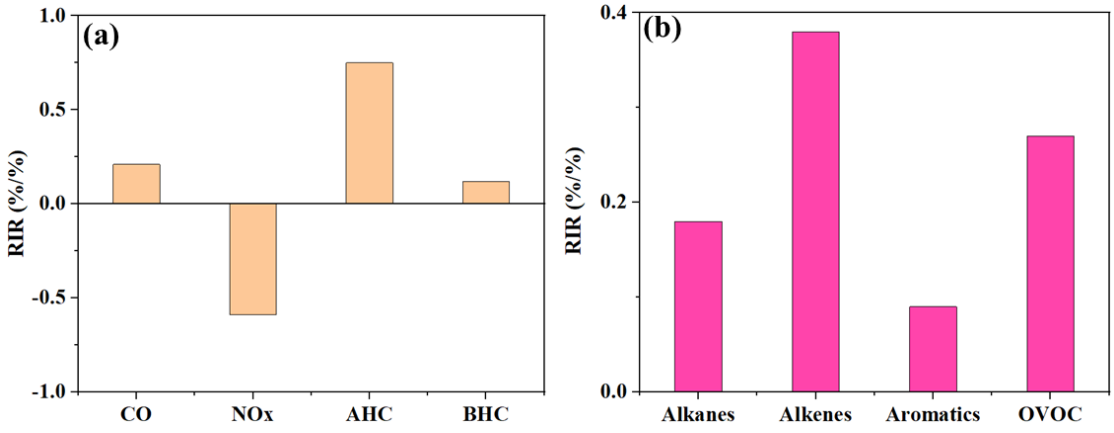

Figure 9 Reduction percentage of O_3 as a function of the reduction percentage of VOCs (a); increase percentage of O_3 as a function of the reduction percentage of NO_x (b).

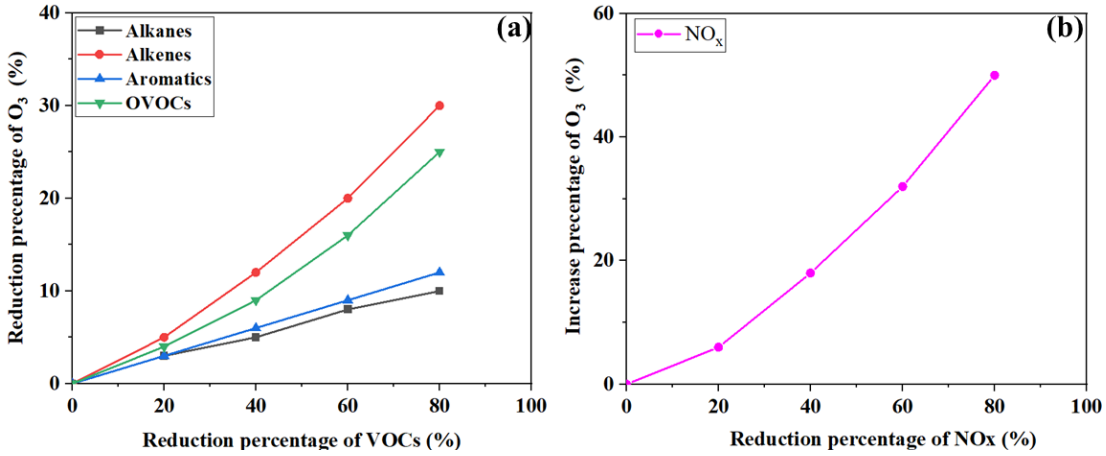

Supplementary Information

Title: Elucidating the mechanisms of rapid O_3 increase in North China Plain during COVID-19 lockdown period

Authors: Rui Li[a *], Yining Gao[a], Gehui Wang[a **]

Affiliations: [a] *Key Laboratory of Geographic Information Science of the Ministry of Education, School of Geographic Sciences, East China Normal University, Shanghai, 200241, PR China*

*** Corresponding author**

R. Li (rli@geo.ecnu.edu.cn) and G. H. Wang (ghwang@geo.ecnu.edu.cn)

Number of pages: 8

Number of figures: 4

Number of tables: 2

Figure S1 The topographic map of China reflecting the location of Tangshan (a), diamond sampling site (b). The yellow circles represent some key sampling sites.

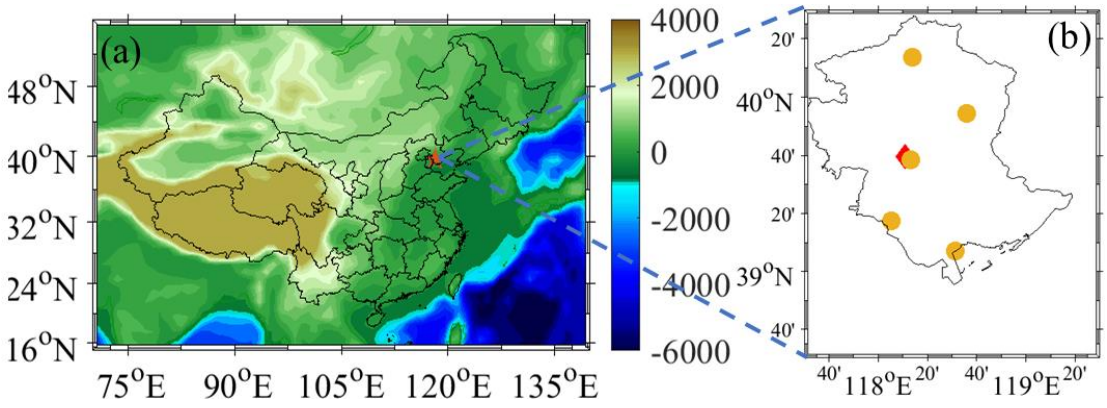

Figure S2 Diurnal patterns of gaseous pollutants and meteorological parameters during the whole period in Tangshan. The error bar is the standard error.

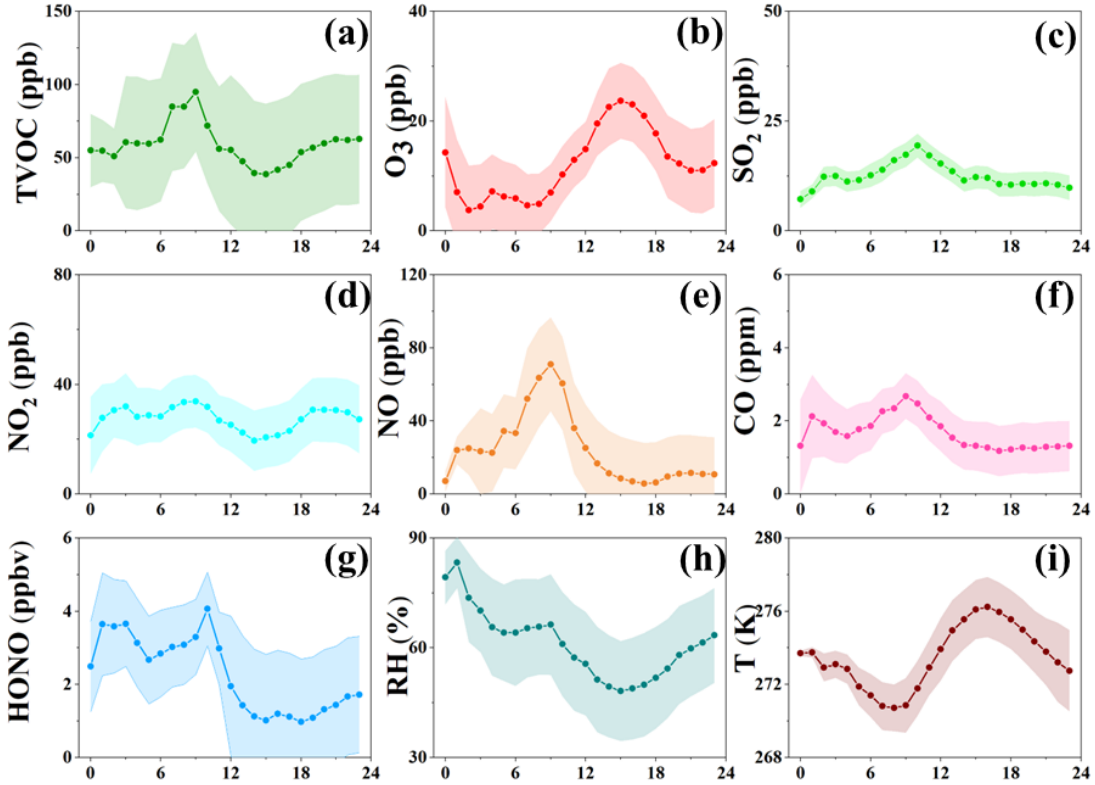

Figure S3 Response curves of O_3 concentration to changes in (a) air temperature (T), (b) relative humidity (RH), (c) pressure (P), and (d) wind speed (WS). The y axis denotes the smoothing function values. The x axis represents the meteorological parameter. The vertical short lines denote the concentration distribution characteristics of the meteorological parameters, and the shaded area around the solid line reflects the 95 % confidence interval of O_3 concentration.

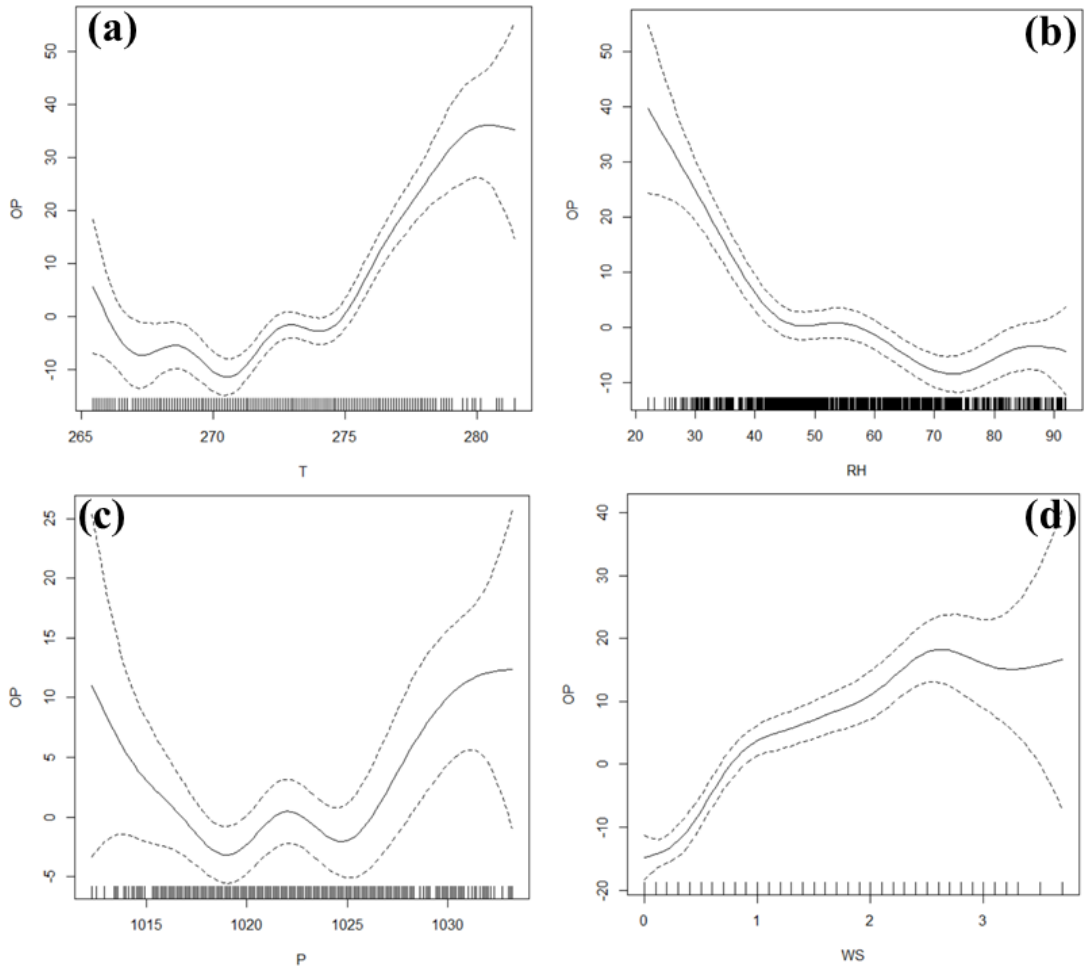

Figure S4 The contribution of HO_2+NO to O_3 formation without aerosol module and with aerosol module before (a) and after lockdown (b).

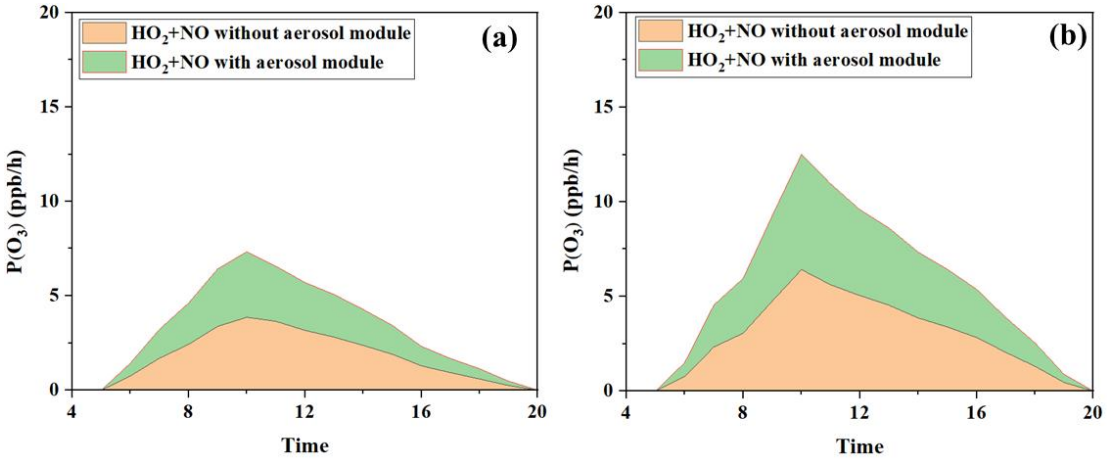

Table S1 All of measured VOC species in our study used to assess the O_3 budget.

VOC species	Classification
toluene	Aromatics
m/p-xylene	Aromatics
o-xylene	Aromatics
benzene	Aromatics
ethylbenzene	Aromatics
styrene	Aromatics
1,2,4-trimethylbenzene	Aromatics
ethyltoluene	Aromatics
isopropylbenzene	Aromatics
1,3,5-trimethylbenzene	Aromatics
1,2,3-trimethylbenzene	Aromatics
n-propylbenzene	Aromatics
dichloromethane	Other VOC species
1,2-dichloroethane	Other VOC species
chloromethane	Other VOC species
1,2-dichloropropane	Other VOC species
bromomethane	Other VOC species
trichloroethene	Other VOC species
acetylene	Other VOC species
acetone	OVOCs
2-butanone	OVOCs
2-propanol	OVOCs
acrolein	OVOCs
2-methoxy-2-methylpropane	OVOCs
2-hexanone	OVOCs
ethane	Alkanes
propane	Alkanes
isopentane	Alkanes
n-butane	Alkanes
n-dodecane	Alkanes
n-pentane	Alkanes
n-hexane	Alkanes
isobutane	Alkanes
n-heptane	Alkanes
3-methylhexane	Alkanes
3-methylpentane	Alkanes
2-methylhexane	Alkanes
2-methylpentane	Alkanes
2,3-dimethylbutane	Alkanes
cyclohexane	Alkanes
n-undecane	Alkanes
n-octane	Alkanes

n-nonane	Alkanes
n-decane	Alkanes
ethene	Alkenes
propene	Alkenes
isoprene	Alkenes
trans-2-pentene	Alkenes
cis-2-butene	Alkenes
1-butene	Alkenes
1-pentene	Alkenes
1-hexane	Alkenes
1,3-butadiene	Alkenes
trans-2-butene	Alkenes

Table S2 Comparison of meteorological parameters before and after COVID-19 lockdown.

Periods	T	RH	P	WS
Pre-lockdown	273	58.4	1019	0.91
Lockdown	273	60.4	1023	1.26